

Cryogenic performance of field-effect transistors and amplifiers based on selective area grown InAs nanowires

Giulia Meucci^{*,1}, Dags Olšteins¹, Damon J. Carrad¹, Gunjan Nagda¹, Daria V. Beznasyuk¹, Christian E. N. Petersen¹, Sara Martí-Sánchez², Jordi Arbiol^{2,3} and Thomas Sand Jespersen^{1,4}

¹*Department of Energy Conversion and Storage, Technical University of Denmark, 2800 Kgs.Lyngby, Denmark*

²*Catalan Institute of Nanoscience and Nanotechnology (ICN2), CSIC and BIST, Campus UAB, Bellaterra, Barcelona, Catalonia, Spain*

³*ICREA, Passeig de Lluís Companys 23, 08010 Barcelona, Catalonia, Spain*

⁴*Center For Quantum Devices, Niels Bohr Institute, University of Copenhagen, 2100 Copenhagen, Denmark*

(*Electronic mail: giuliam@dtu.dk)

(Dated: 3 September 2025)

Indium-Arsenide (InAs) nanowire field-effect transistors (NWFETs) are promising platforms for high-speed, low-power nanoelectronics operating at cryogenic conditions, relevant for quantum information processing. We present selective area growth (SAG) of nanowires, which enable scalability and planar geometries that are compatible with standard semiconductor processing techniques. NWFETs are fabricated and their low temperature characteristics - including $I_{\text{ON}}/I_{\text{OFF}}$ ratios, threshold voltages, sub-threshold slope, interfacial trap density, hysteresis, and mobility - are characterized. The NWFETs operate successfully in integrated circuitry relying on saturation-mode operation. In sub-threshold applications such as amplifiers, we find bandwidths exceeding our cryostat wiring, but the gate hysteresis presents challenges for precise tuning of the amplifier operating point. We discuss the role of crystal imperfections and fabrication processes on the transistor characteristics and propose strategies for further improvements.

The prospects of large-scale electronic quantum circuits motivate the continuous search for optimal, scalable, and reproducible material platforms for mesoscopic devices. Selective area growth (SAG) of semiconductor nanowires^{1–3} offers an interesting approach by adding scalability to the nanowire platform, which has already proven successful at the single-device prototype level, both as active elements in high-performance field-effect transistors (FETs) at cryogenic conditions^{4–15} and for advanced quantum devices^{16–19}.

Nanowires are traditionally grown by the vapor-liquid-solid (VLS) mechanism²⁰ which results in an out-of-plane growth incompatible with standard semiconductor processing. Thus, laborious and irreproducible manual methods^{21–23}, are employed for transferring VLS nanowires to suitable device substrates, which has prevented the up-scaling of nanowire circuits. In contrast, SAG allows lithographic control of in-plane growth of single nanowires and nanowire networks and thus opens a route towards scalable nanoelectronics^{1,2,24–27}.

Unlike VLS-grown nanowires, planar selective area grown nanowires are epitaxially clamped to the substrate along their length, and crystal growth occurs over a much larger front. This makes the basic growth mechanism qualitatively different²⁸, increases the susceptibility to misfit dislocations and material intermixing^{29,30}, and also requires device fabrication directly on the growth substrate. These factors may potentially compromise the electrical performance of selective area grown nanowires and devices. Here we present fabrication, measurements, and detailed analysis of InAs selective area grown NWFETs and explore their performance in amplifier circuits at cryogenic conditions relevant for applications in integrated control electronics for quantum circuits.

In-plane SAG of InAs nanowires was performed by

molecular beam epitaxy (MBE) using insulating GaAs (311) substrates which were first covered with 10nm of SiO₂ by plasma-enhanced chemical vapor deposition. Subsequently the GaAs surface was re-exposed in $0.15 \times 10 \mu\text{m}$ nanowire-shaped regions along the [011] direction using electron beam lithography and CF₄ plasma etching. The surface was prepared for the InAs growth by annealing at 610°C to remove native oxides followed by selective growth of a GaAs(Sb) buffer layer²⁴ (see Fig. 1a). A cross-section high-angle annular dark-field scanning transmission micrograph (HAADF STEM) of a typical nanowire is shown in Fig. 1b. Details of growth and structural analysis is reported elsewhere^{24,31}. FETs with Ti/Au ohmic contacts and a source-drain separation of $1 \mu\text{m}$ were fabricated directly on the growth substrate and included a top-gate separated from the nanowire by 15nm of HfO₂ grown by atomic layer deposition. Typical devices are shown in Fig. 1c. The devices were incorporated into an on-chip multiplexer circuit, as described in Ref. 24, and here we analyze the details of individual FET devices. The NWFETs were characterized by measuring the dependence of the source-drain current, I_{SD} , on the source-drain voltage, V_{SD} (output characteristics), and on the gate voltage, V_{G} (transfer characteristics), at temperatures down to $T = 14$ mK, in a dilution cryostat. In total, eight identical devices (D1-D8) were studied. An overview of the characterization parameters for each device can be found in supplementary section S1. Device D8 showed effects of quantum interference and ballistic transport at low temperature and low bias (supplementary section S2), and was excluded from the analysis of FET parameters. The main text shows representative data and additional results are presented in the supplementary material.

Figure 1d shows the output characteristics of D1, measured

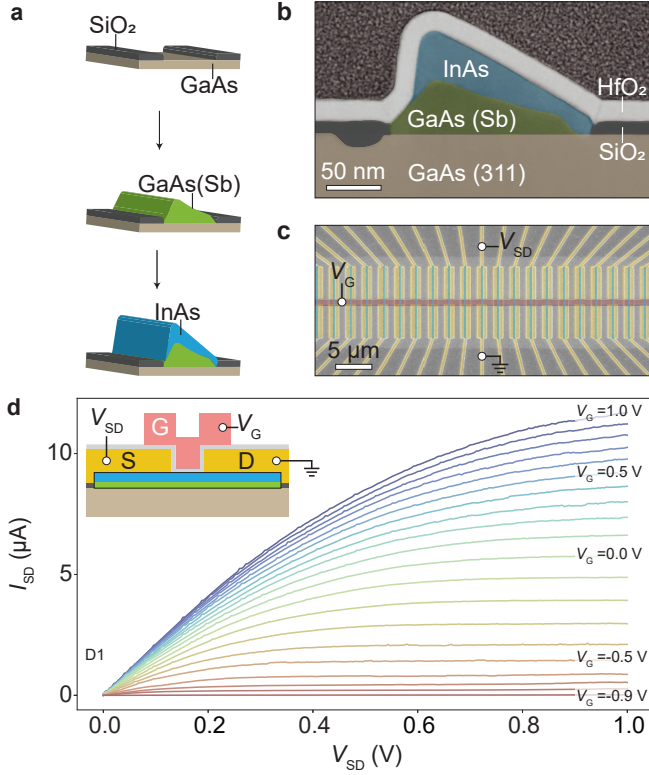


FIG. 1. **a** Schematic illustration of SAG of InAs nanowires. **b** False-color HAADF STEM micrograph showing the cross section of a typical nanowire. **c** False-color SEM micrograph of planar selective area grown nanowire transistors. Each nanowire has individual Ti/Au source-drain contacts (yellow) and all devices share a common top gate (pink). **d** Output characteristics of device D1 at 9 K with V_G ranging from -0.9 V (red) to 1.0 V (blue), in steps of 0.1 V. The inset shows a schematic of the device layout.

at 9 K, for V_G ranging between -0.9 and 1 V. An ohmic regime is observed at low V_{SD} , followed by a saturation regime at higher bias, consistent with previous results for InAs NWFETs at room temperature^{6–8,11,12,14,15}, demonstrating that the selective area grown device acts as a classical FET even in the cryogenic limit.

Figures 2a,b show the transfer characteristics of D4, measured at 14 mK, for values of V_{SD} between 20 and 100 mV, in linear and logarithmic scale, respectively. Similar measurements for other devices are presented in supplementary section S2. Due to limited measurement sensitivity in the sub-nanoampere range the current saturates at low V_G to a bias-independent value of ~ 0.35 nA, which serves as an upper bound on the off-state current, I_{OFF} , while the ON current, I_{ON} , is defined as the current at the highest V_G . Based on the $V_{SD} = 100$ mV transfer characteristics the corresponding lower bound on the I_{ON}/I_{OFF} ratio is then 5×10^3 . This value is lower, and thus consistent, compared to those reported for VLS InAs FETs¹⁰ and further experiments are needed to determine and quantify any significant differences between the two growth methods.

To estimate the threshold voltage, V_{th} , we follow the

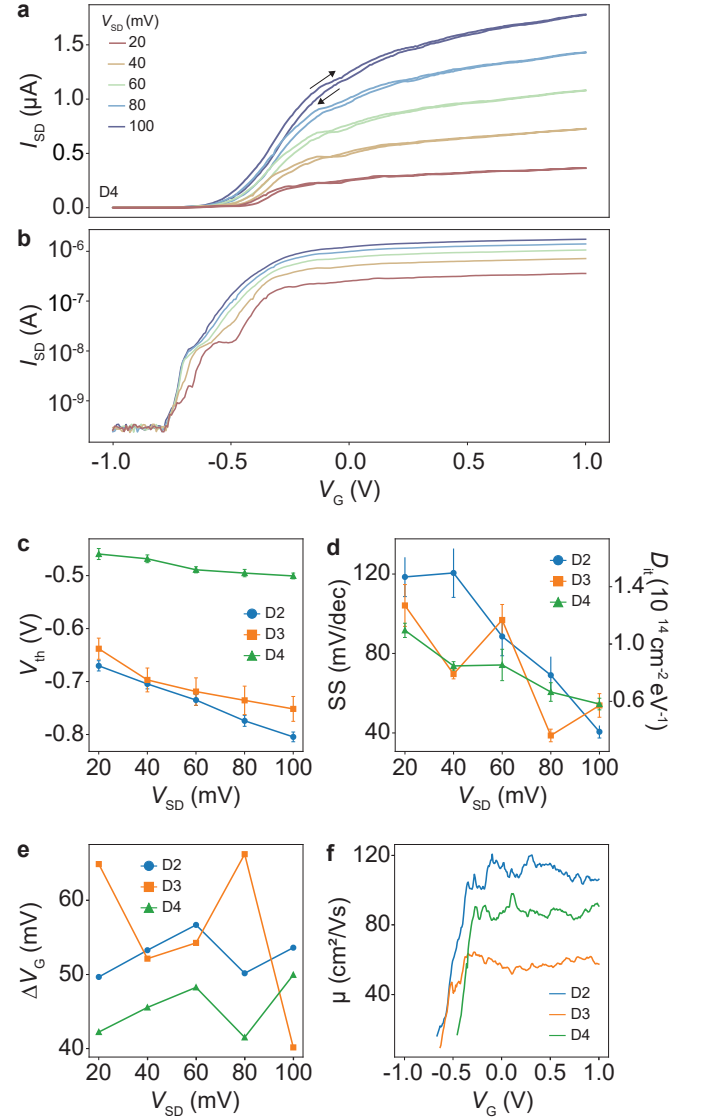


FIG. 2. **a** Transfer characteristics of D4 measured at 14 mK for V_{SD} ranging from 20 mV (red) to 100 mV (blue) in steps of 20 mV. **b** Curves with positive sweep direction from panel **a** shown on logarithmic scale. **c**, **d**, **e**, **f** Bias dependence of the lower bound of the I_{ON}/I_{OFF} ratio (**c**), threshold voltage (**d**), inverse sub-threshold slope and associated density of interfacial charge traps (**e**), and gate hysteresis (**f**). **g** V_G -dependence of the field effect mobility at $V_{SD} = 20$ mV.

method outlined in Ref. 32 (see supplementary section S3). The results are shown in Fig. 2c as a function of V_{SD} . For all devices, a negative V_{th} is observed, which shows that the devices act as n -type depletion mode FETs, as expected since nominally undoped InAs forms an electron accumulation layer at the surface, shifting the Fermi level above the conduction band edge³³. Moreover, V_{th} decreases with V_{SD} , indicating significant drain-induced barrier lowering (DIBL) of 1.7 ± 0.2 , 1.3 ± 0.4 , and 0.5 ± 0.1 V/V for devices D2, D3, and D4, respectively. These values are consistent with those reported for InAs NWFET with similar architecture

and aspect ratios³⁴. Lower values may be obtained through optimized device designs^{5,35,36}.

As shown in Fig. 2b, I_{SD} exhibits an exponential increase with V_G for $V_G < V_{th}$, as expected for FETs. To analyze this sub-threshold regime the transfer characteristics were fitted to the standard expression $I_{SD} = I_{OFF} \times 10^{(V_G - V_t)/SS}$, where V_t and the inverse sub-threshold slope, SS , are fitting parameters³⁷. We take the fitting range extending from the highest V_G where $I_{SD} < I_{OFF} + 10^{-11}$ A to the lowest V_G where $I_{SD} > I_{OFF} \times 10^2$. This convention allows consistent examination of the sub-threshold region for the different devices. Figure 2d shows the resulting SS for different devices and V_{SD} . SS falls within the range 40 – 120 mV/decade similar to reported values for top-gated InAs NWFETs^{13,34,38–41}. In the cryogenic limit we expect $SS \approx W_t \ln(10)(1 + e^2 D_{it} A_G / C_G) / e$, where $W_t \approx 5.7$ meV is the characteristic decay of the conduction band tail in the bandgap^{42,43}, C_G is the gate capacitance, A_G is the gate area, and D_{it} is the density of charge traps at the InAs/HfO₂ interface, reducing the effectiveness of the gate. The devices here have $A_G = 180 \text{ nm} \times 1 \mu\text{m}$, and $C_G = 5.3$ fF was determined by numerical simulations²⁴. With these values we find $D_{it} \sim 10^{14} \text{ cm}^{-2} \text{ eV}^{-1}$ (Fig. 2d), one order of magnitude lower than values reported for back-gated InAs VLS NWFETs⁴⁴ while an order higher than reported for optimized top gated devices^{5,13}. This suggests that our selective area grown devices can be further improved by systematic optimization of the oxide/nanowire interface⁴⁵.

The presence of interfacial charge traps is consistent with the up/down V_G sweep hysteresis of the transfer curves³¹, observed in Fig. 2a. To quantify the hysteresis, we estimate the voltage shift, ΔV_G , between the up and down sweep curves (see supplementary section S4 for details). As shown in Fig. 2e ΔV_G ranges from 40 to 60 mV which is significantly lower than the typical width of the transfer characteristics, $\sim 150 - 600$ mV, estimated from the width of a Lorentzian fit to the peaked trans-conductance dI_{SD}/dV_G . This enables the use of the NWFETs in circuitry requiring switching and saturation, such as multiplexers²⁴ or other key components in integrated control electronics. The role of hysteresis in sub-threshold applications, like amplifiers, is discussed below.

To complete the electrical characterization, the mobility, μ , of the NWFETs is assessed based on the $V_{SD}=20$ mV data following the procedure outlined in Ref. 32 (see supplementary section S3). As shown in Fig. 2f μ remains almost constant for $V_G > V_{th}$, with values in the range 60-120 cm^2/Vs . The μ values are lower compared to other reported InAs nanowires, grown using both VLS^{6–10,12,15,46} and SAG^{2,25,36}. We attribute this difference to the growth limitations discussed above. We expect that substantial enhancements of μ can be obtained, for example, by including an InGaAs buffer layer in the selective area grown nanowire heterostructure, as demonstrated in Ref. 29.

Having established the overall characteristics of the InAs selective area grown NWFETs, we now consider their performance in the common source amplifier configuration shown in Fig. 3a, with a NWFET operating at 7.5 K. Figure 3b shows the amplifier output voltage, V_{out} , for various bias

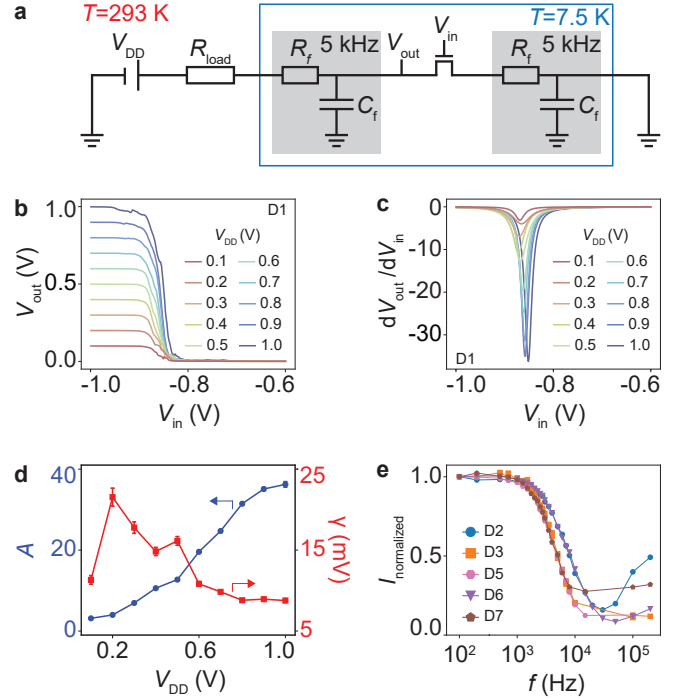


FIG. 3. **a** Common source amplifier circuit. The selective area grown NWFET (D1) is kept at 7.5 K and the 100 M Ω load resistor at room temperature. **b** Amplifier output, V_{out} , as a function of input, V_{in} , and bias voltage, V_{DD} . **c** Lorentzian fits of the derivative of the curves in panel (b). **d** Lorentzian's amplitude, A (amplification), and half width, γ , as a function of bias. **e** Normalized frequency response of different NWFETs to a sinusoidal V_G of frequency f , measured at 1.2 K.

levels, V_{DD} , as a function of the input voltage, V_{in} , applied to the gate. The circuit operates as an inverting amplifier, as a positive change in V_{in} results in a negative change in V_{out} . The amplification A is determined as the peak amplitude in dV_{out}/dV_{in} , which was fitted to a Lorentzian line shape as shown in Fig. 3c. The amplitudes and characteristic peak widths, $2\gamma = \text{FWHM}$, are shown in Fig. 3d as a function of V_{DD} . The maximum voltage gain ~ 36 is obtained at the highest V_{DD} and optimal gate-operation point $V_0 \approx -0.86$ V. Upon shifting the operating point from V_0 by γ the gain is reduced by a factor 2 and at high V_{DD} we find $\gamma \sim 10$ mV which is significantly smaller than the typical hysteresis $\Delta V_G \sim 50$ mV (Fig. 2f). This shows that for sub-threshold applications, such as amplifiers, the NWFET hysteresis should be reduced. Taking steps to improve the oxide and oxide/nanowire interface quality is likely to yield devices suitable for such applications.

Due to the high mobility, InAs is often used in high bandwidth applications¹⁵ and Fig. 3e shows the normalized current response of isolated NWFETs subject to a sinusoidal gate modulation of frequency f (see supplementary section S5 and S6). For all devices, a cutoff frequency ~ 5 kHz, is found, matching the 5 kHz cutoff of the cryostat filtering. This shows that, despite the relatively low mobility and

significant interface charge trapping, the cutoff frequency of the NWFET exceeds this limit. Further measurements performed in a cryogenic high-bandwidth environment are needed to establish the upper operational limit.

In summary, we have reported the fabrication and electrical characterization at cryogenic temperature of FETs based on InAs nanowires realized by selective area MBE. The devices act as *n*-type depletion mode FETs, with $I_{\text{ON}}/I_{\text{OFF}}$ ratio exceeding 10^3 , DIBL between 0.5 and 1.7 V/V and mobility ranging from 60 to 120 cm^2/Vs . The current-voltage characteristics exhibit hysteresis during gate sweeps and sub-threshold analysis reveals a density of interfacial traps on the order of $10^{14} \text{ cm}^{-2} \text{ eV}^{-1}$. The modest transistor characteristics could be improved by optimizing the nanowire growth to reduce misfit dislocations and material intermixing²⁹. Furthermore, we tested the NWFETs in a common source amplifier configuration exhibiting a maximum amplification of 36 at $V_{\text{DD}} = 1 \text{ V}$, and we observed a NWFET bandwidth higher than that of the cryogenic setup. Overall, the NWFETs operate successfully in saturation-mode applications, while the hysteresis remains a limitation for sub-threshold operations. Taken all together, however, the results demonstrate the potential of InAs selective area grown NWFETs for scalable high-frequency cryogenic nanoelectronics.

See the supplementary material for detailed information on the performed measurements, additional transfer characteristics data, the methodology used to extract threshold voltage and mobility, details on hysteresis computations and on bandwidth measurements in both the amplifier and NWFET configurations.

ACKNOWLEDGMENTS

This work was supported by the European Research Council under the European Union's Horizon 2020 research and innovation program (Grant no.: 866158). ICN2 acknowledges funding from Generalitat de Catalunya 2021SGR00457. Authors acknowledge the Advanced Materials programme by the Spanish Government with funding from European Union NextGenerationEU (PRTR-C17.I1) and by Generalitat de Catalunya (In-CAEM Project). We acknowledge support from CSIC Interdisciplinary Thematic Platform (PTI+) on Quantum Technologies (PTI-QTEP+). This research work has been funded by the European Commission – NextGenerationEU (Regulation EU 2020/2094), through CSIC's Quantum Technologies Platform (QTEP). ICN2 is supported by the Severo Ochoa program from Spanish MCIN / AEI (Grant No.: CEX2021-001214-S) and is funded by the CERCA Programme / Generalitat de Catalunya. Authors acknowledge the use of instrumentation as well as the technical advice provided by the Joint Electron Microscopy Center at ALBA (JEMCA). ICN2 acknowledges funding from Grant IU16-014206 (METCAM-FIB) funded by the European Union through the European Regional Development Fund (ERDF), with the support of the Ministry of Research and Universities, Generalitat de Catalunya. ICN2 is founding member of e-DREAM.

AUTHOR DECLARATIONS

Conflict of Interest

The authors have no conflicts to disclose.

Author Contributions

Giulia Meucci: Formal analysis; Methodology; Visualization; Writing – original draft; Writing – review & editing. **Dags Olšteins:** Conceptualization; Data curation; Investigation; Writing – review & editing. **Damon J. Carrad:** Conceptualization; Data curation; Investigation; Writing – review & editing. **Gunjan Nagda:** Data curation; Investigation; Writing – review & editing. **Daria V. Beznasyuk:** Data curation; Investigation; Writing – review & editing. **Christian E. N. Petersen:** Methodology; Writing – review & editing. **Sara Martí-Sánchez:** Data curation; Investigation. **Jordi Arbiol:** Data curation; Investigation. **Thomas Sand Jespersen:** Conceptualization; Supervision; Project administration; Writing – original draft; Writing – review & editing.

DATA AVAILABILITY

The data that support the findings of this study are openly available at <https://doi.org/10.11583/DTU.29859029>.

REFERENCES

- ¹M. Friedl, K. Cerveny, P. Weigle, G. Tütüncüoglu, S. Martí-Sánchez, C. Huang, T. Patlatiuk, H. Potts, Z. Sun, M. O. Hill, L. Güniat, W. Kim, M. Zamani, V. G. Dubrovskii, J. Arbiol, L. J. Lauhon, D. M. Zumbühl, and A. Fontcuberta i Morral, “Template-Assisted Scalable Nanowire Networks,” *Nano Lett.* **18**, 2666–2671 (2018).
- ²F. Krizek, J. E. Sestoft, P. Aseev, S. Martí-Sánchez, S. Vaitiekėnas, L. Casparis, S. A. Khan, Y. Liu, T. Stankevič, A. M. Whitticar, *et al.*, “Field effect enhancement in buffered quantum nanowire networks,” *Phys. Rev. Mater.* **2**, 093401 (2018).
- ³S. Vaitiekėnas, A. M. Whitticar, M.-T. Deng, F. Krizek, J. E. Sestoft, C. J. Palmström, S. Martí-Sánchez, J. Arbiol, P. Krogstrup, L. Casparis, and C. M. Marcus, “Selective-Area-Grown Semiconductor-Superconductor Hybrids: A Basis for Topological Networks,” *Phys. Rev. Lett.* **121**, 147701 (2018).
- ⁴J. A. Del Alamo, “Nanometre-scale electronics with III–V compound semiconductors,” *Nature* **479**, 317–323 (2011).
- ⁵C. Zhang and X. Li, “III–V nanowire transistors for low-power logic applications: a review and outlook,” *IEEE Trans. Electron Devices* **63**, 223–234 (2016).
- ⁶A. W. Dey, C. Thelander, E. Lind, K. A. Dick, B. M. Borg, M. Borgström, P. Nilsson, and L.-E. Wernersson, “High-performance InAs nanowire MOSFETs,” *IEEE Electron Device Lett.* **33**, 791–793 (2012).
- ⁷A. C. Ford, J. C. Ho, Y.-L. Chueh, Y.-C. Tseng, Z. Fan, J. Guo, J. Bokor, and A. Javey, “Diameter-Dependent Electron Mobility of InAs Nanowires,” *Nano Lett.* **9**, 360–365 (2009).
- ⁸S. Sasaki, K. Tateno, G. Zhang, H. Suominen, Y. Harada, S. Saito, A. Fujiwara, T. Sogawa, and K. Muraki, “Encapsulated gate-all-around InAs nanowire field-effect transistors,” *App. Phys. Lett.* **103** (2013).
- ⁹S. A. Dayeh, E. T. Yu, and D. Wang, “Transport coefficients of InAs nanowires as a function of diameter,” *Small* **5**, 77–81 (2009).
- ¹⁰K. Storm, G. Nylund, L. Samuelson, and A. P. Micolich, “Realizing lateral wrap-gated nanowire FETs: controlling gate length with chemistry rather than lithography,” *Nano Lett.* **12**, 1–6 (2012).
- ¹¹H. A. Nilsson, P. Caroff, C. Thelander, E. Lind, O. Karlström, and L.-E. Wernersson, “Temperature dependent properties of InSb and InAs nanowire field-effect transistors,” *Appl. Phys. Lett.* **96** (2010).
- ¹²S. Dhara, S. Sengupta, H. S. Solanki, A. Maurya, A. Pavan R, M. Gokhale, A. Bhattacharya, and M. M. Deshmukh, “Facile fabrication of lateral nanowire wrap-gate devices with improved performance,” *Appl. Phys. Lett.* **99** (2011).

- ¹³Y. Jiang, R. Shen, T. Li, J. Tian, S. Li, H. H. Tan, C. Jagadish, and Q. Chen, "Enhancing the electrical performance of InAs nanowire field-effect transistors by improving the surface and interface properties by coating with thermally oxidized Y_2O_3 ," *Nanoscale* **14**, 12830–12840 (2022).
- ¹⁴L. E. Froberg, C. Rehnstedt, C. Thelander, E. Lind, L.-E. Wernersson, and L. Samuelson, "Heterostructure barriers in wrap gated nanowire FETs," *IEEE Electron Device Lett.* **29**, 981–983 (2008).
- ¹⁵K. Blekker, B. Munstermann, A. Matiss, Q. T. Do, I. Regolin, W. Brockerhoff, W. Prost, and F.-J. Tegude, "High-frequency measurements on InAs nanowire field-effect transistors using coplanar waveguide contacts," *IEEE Trans. Nanotechnol.* **9**, 432–437 (2010).
- ¹⁶L. Hofstetter, S. Csonka, J. Nygård, and C. Schönenberger, "Cooper pair splitter realized in a two-quantum-dot Y-junction," *Nature* **461**, 960–963 (2009).
- ¹⁷T. S. Jespersen, M. Aagesen, C. B. Sørensen, P. E. Lindelof, and J. Nygård, "Tunable double dots and Kondo enhanced Andreev transport in InAs nanowires," *J. Vac. Sci. Technol. B Microelectron. Nanometer Struct. Process. Meas. Phenom.* **26**, 1609 (2008).
- ¹⁸T. W. Larsen, K. D. Petersson, F. Kuemmeth, T. S. Jespersen, P. Krogstrup, J. Nygård, and C. M. Marcus, "Semiconductor-Nanowire-Based Superconducting Qubit," *Phys. Rev. Lett.* **115**, 127001 (2015).
- ¹⁹S. Nadj-Perge, S. M. Frolov, E. P. A. M. Bakkers, and L. P. Kouwenhoven, "Spin-orbit qubit in a semiconductor nanowire," *Nature* **468**, 1084–1087 (2010).
- ²⁰a. R. Wagner and s. W. Ellis, "Vapor-liquid-solid mechanism of single crystal growth," *Appl. Phys. Lett.* **4**, 89–90 (1964).
- ²¹E. M. Freer, O. Grachev, X. Duan, S. Martin, and D. P. Stumbo, "High-yield self-limiting single-nanowire assembly with dielectrophoresis," *Nature Nanotech* **5**, 525–530 (2010).
- ²²J. Yao, H. Yan, and C. M. Lieber, "A nanoscale combing technique for the large-scale assembly of highly aligned nanowires," *Nature Nanotech* **8**, 329–335 (2013).
- ²³M. Fu, "Fabrication, Characterization and Parameter Extraction of InAs Nanowire-Based Device," in *Electrical Properties of Indium Arsenide Nanowires and Their Field-Effect Transistors*, Springer Theses, edited by M. Fu (Singapore, 2018) pp. 31–51.
- ²⁴D. Olšteins, G. Nagda, D. J. Carrad, D. V. Beznasyuk, C. E. N. Petersen, S. Martí-Sánchez, J. Arbiol, and T. S. Jespersen, "Cryogenic multiplexing using selective area grown nanowires," *Nat Commun* **14**, 7738 (2023).
- ²⁵M. Friedl, K. Cerveny, C. Huang, D. Dede, M. Samani, M. O. Hill, N. Morgan, W. Kim, L. Guniat, J. Segura-Ruiz, *et al.*, "Remote doping of scalable nanowire branches," *Nano Lett.* **20**, 3577–3584 (2020).
- ²⁶R. L. M. Op het Veld, D. Xu, V. Schaller, M. A. Verheijen, S. M. E. Peters, J. Jung, C. Tong, Q. Wang, M. W. A. de Moor, B. Hesselmann, K. Vermeulen, J. D. S. Bommer, J. Sue Lee, A. Sarikov, M. Pendharkar, A. Marzegalli, S. Koelling, L. P. Kouwenhoven, L. Miglio, C. J. Palmstrøm, H. Zhang, and E. P. A. M. Bakkers, "In-plane selective area InSb–Al nanowire quantum networks," *Commun. Phys.* **3**, 1–7 (2020).
- ²⁷L. Södergren, P. Olsson, and E. Lind, "Low-Temperature Characteristics of Nanowire Network Demultiplexer for Qubit Biasing," *Nano Lett.* **22**, 3884–3888 (2022).
- ²⁸D. V. Beznasyuk, S. Martí-Sánchez, G. Nagda, D. J. Carrad, J. Arbiol, and T. S. Jespersen, "Scale-dependent growth modes of selective area grown III–V nanowires," *Nano letters* **24**, 14198–14205 (2024).
- ²⁹D. V. Beznasyuk, S. Martí-Sánchez, J.-H. Kang, R. Tanta, M. Rajpalke, T. Stankevič, A. W. Christensen, M. C. Spadaro, R. Bergamaschini, N. N. Maka, C. E. N. Petersen, D. J. Carrad, T. S. Jespersen, J. Arbiol, and P. Krogstrup, "Doubling the mobility of InAs/InGaAs selective area grown nanowires," *Phys. Rev. Materials* **6**, 034602 (2022).
- ³⁰F. Krizek, J. E. Sestoft, P. Aseev, S. Marti-Sanchez, S. Vaitiekėnas, L. Casparis, S. A. Khan, Y. Liu, T. Stankevič, A. M. Whitticar, A. Fursina, F. Boekhout, R. Koops, E. Uccelli, L. P. Kouwenhoven, C. M. Marcus, J. Arbiol, and P. Krogstrup, "Field effect enhancement in buffered quantum nanowire networks," *Phys. Rev. Materials* **2**, 093401 (2018).
- ³¹D. Olšteins, G. Nagda, D. J. Carrad, D. V. Beznasyuk, C. E. N. Petersen, S. Martí-Sánchez, J. Arbiol, and T. S. Jespersen, "Statistical Reproducibility of Selective Area Grown InAs Nanowire Devices," *Nano Lett.* **24**, 6553–6559 (2024).
- ³²C. E. Petersen, D. J. Carrad, T. Désiré, D. Beznasyuk, J.-H. Kang, D. Olšteins, G. Nagda, D. V. Christensen, and T. S. Jespersen, " $\mu_{2T}(n)$: A method for extracting the density dependent mobility in two-terminal nanodevices," *arXiv preprint arXiv:2508.06173* (2025).
- ³³L. Olsson, C. Andersson, M. Håkansson, J. Kanski, L. Ilver, and U. O. Karlsson, "Charge accumulation at InAs surfaces," *Phys. Rev. Lett.* **76**, 3626 (1996).
- ³⁴W. Yang, D. Pan, R. Shen, X. Wang, J. Zhao, and Q. Chen, "Suppressing the excess OFF-state current of short-channel InAs nanowire field-effect transistors by nanoscale partial-gate," *Nanotechnology* **29**, 415203 (2018).
- ³⁵K. Tomioka, M. Yoshimura, and T. Fukui, "A III–V nanowire channel on silicon for high-performance vertical transistors," *Nature* **488**, 189–192 (2012).
- ³⁶K. Tomioka, F. Izhizaka, and T. Fukui, "Selective-area growth of InAs nanowires on Ge and vertical transistor application," *Nano Lett.* **15**, 7253–7257 (2015).
- ³⁷S. M. Sze, Y. Li, and K. K. Ng, *Physics of semiconductor devices* (John Wiley & sons, 2021).
- ³⁸T. Vasen, P. Ramvall, A. Afzal, C. Thelander, K. Dick, M. Holland, G. Doornbos, S. Wang, R. Oxland, G. Vellianitis, M. van Dal, B. Duriez, J.-R. Ramirez, R. Droopad, L.-E. Wernersson, L. Samuelson, T.-K. Chen, Y.-C. Yeo, and M. Passlack, "InAs nanowire GAA n-MOSFETs with 12–15 nm diameter," in *2016 IEEE Symp. VLSI Technol.* (2016) pp. 1–2.
- ³⁹C. Zhang, W. Choi, P. K. Mohseni, and X. Li, "InAs Planar Nanowire Gate-All-Around MOSFETs on GaAs Substrates by Selective Lateral Epitaxy," *IEEE Electron Device Lett.* **36**, 663–665 (2015).
- ⁴⁰M. Fu, D. Pan, Y. Yang, T. Shi, Z. Zhang, J. Zhao, H. Q. Xu, and Q. Chen, "Electrical characteristics of field-effect transistors based on indium arsenide nanowire thinner than 10 nm," *Applied Physics Letters* **105**, 143101 (2014).
- ⁴¹Q. Li, S. Huang, D. Pan, J. Wang, J. Zhao, and H. Q. Xu, "Suspended InAs nanowire gate-all-around field-effect transistors," *Applied Physics Letters* **105**, 113106 (2014).
- ⁴²A. Beckers, F. Jazaeri, and C. Enz, "Theoretical limit of low temperature subthreshold swing in field-effect transistors," *IEEE Electron Device Lett.* **41**, 276–279 (2019).
- ⁴³P. Sarangapani, Y. Chu, J. Charles, G. Klimeck, and T. Kubis, "Band-tail formation and band-gap narrowing driven by polar optical phonons and charged impurities in atomically resolved III–V semiconductors and nanodevices," *Phys. Rev. Appl.* **12**, 044045 (2019).
- ⁴⁴T. Li, R. Shen, M. Sun, D. Pan, J. Zhang, J. Xu, J. Zhao, and Q. Chen, "Improving the electrical properties of InAs nanowire field effect transistors by covering them with $\text{Y}_2\text{O}_3/\text{HfO}_2$ layers," *Nanoscale* **10**, 18492–18501 (2018).
- ⁴⁵H. Riel, L.-E. Wernersson, M. Hong, and J. A. del Alamo, "III–V compound semiconductor transistors—from planar to nanowire structures," *MRS Bulletin* **39**, 668–677 (2014).
- ⁴⁶N. Wang, X. Yuan, X. Zhang, Q. Gao, B. Zhao, L. Li, M. Lockrey, H. H. Tan, C. Jagadish, and P. Caroff, "Shape engineering of InP nanostructures by selective area epitaxy," *ACS nano* **13**, 7261–7269 (2019).

Supplementary Material for Cryogenic performance of field-effect transistors and amplifiers based on selective area grown InAs nanowires

Giulia Meucci,¹ Dags Olšteins,¹ Damon J. Carrad,¹ Gunjan Nagda,¹ Daria V. Beznasyuk,¹ Christian E. N. Petersen,¹ Sara Martí-Sánchez,² Jordi Arbiol,^{2,3} and Thomas Sand Jespersen^{1,4}

¹*Department of Energy Conversion and Storage, Technical University of Denmark, 2800 Kgs.Lyngby, Denmark*

²*Catalan Institute of Nanoscience and Nanotechnology (ICN2), CSIC and BIST, Bellaterra, Barcelona, Catalonia, Spain*

³*ICREA, Passeig de Lluís Companys 23, 08010 Barcelona, Catalonia, Spain*

⁴*Center For Quantum Devices, Niels Bohr Institute, University of Copenhagen, 2100 Copenhagen, Denmark*

S1. DETAILS OF PERFORMED MEASUREMENTS

Eight nominally identical devices (D1-D8) were measured, with each device having some or all of the following types of characterizations: output characteristics, transfer characteristics, amplifier characteristics, amplifier bandwidth, and transistor bandwidth. Measurements were performed at cryogenic temperatures and voltage ranges indicated in the table below.

Device	Output characteristics I_{SD} vs V_{SD}	Transfer characteristics I_{SD} vs V_G	Amplifier characteristics V_{out} vs V_{in}	Amplifier Bandwidth A vs f	Transistor Bandwidth $I_{normalized}$ vs f
D1	Fig. 1b ^a	Fig. S1 ^b	Fig. 3b ^f	Fig. S5 ^g	
D2		Fig. S2 ^c			Fig. 3e ^h
D3		Fig. S2 ^c			Fig. 3e, S6 ⁱ
D4		Fig. 2a,b ^c			
D5		Fig. S2 ^d			Fig. 3e ^j
D6		Fig. S2 ^d			Fig. 3e ^k
D7		Fig. S2 ^d			Fig. 3e ^l
D8		Fig. S2 ^e			

^a $T = 9$ K, $V_{SD} = 0$ to 1 V, $V_G = -0.9$ to 1 V (steps 0.1 V).

^b $T = 8.5$ K, $V_G = -1$ to 1 V (sweep rate ~ 60 mV/s), $V_{SD} = 0.1$ to 1 V (steps 0.1 V).

^c $T = 14$ mK, $V_G = -1$ to 1 V (sweep rate ~ 60 mV/s), $V_{SD} = 20$ to 100 mV (steps 20 mV).

^d $T = 14$ mK, $V_G = -1$ to 1 V (sweep rate ~ 60 mV/s), $V_{SD} = 100$ mV.

^e $T = 14$ mK, $V_G = -1$ to 0 V (sweep rate ~ 60 mV/s), $V_{SD} = 20$ to 100 mV (steps 20 mV).

^f $T = 7.5$ K, $V_{in} = -1$ to -0.6 V, $V_{DD} = 0.1$ to 1 V (steps 0.1 V).

^g $T = 7.5$ K, $f = 1$ to 10^4 Hz, $V_{DD} = 1$ V, $V_0 = -0.882$ V.

^h $T = 1.2$ K, $f = 10^2$ to $2 \cdot 10^5$ Hz, $V_{SD} = 0.02$ V, $V_{G0} = -0.5$ V.

ⁱ $T = 1.2$ K, $f = 1$ to $2 \cdot 10^5$ Hz, $V_{SD} = 0.1$ V, $V_{G0} = -0.6$ V.

^j $T = 1.2$ K, $f = 10^2$ to $2 \cdot 10^5$ Hz, $V_{SD} = 0.1$ V, $V_{G0} = -0.725$ V.

^k $T = 1.2$ K, $f = 10^2$ to $2 \cdot 10^5$ Hz, $V_{SD} = 0.1$ V, $V_{G0} = -0.65$ V.

^l $T = 1.2$ K, $f = 10^2$ to $2 \cdot 10^5$ Hz, $V_{SD} = 0.1$ V, $V_{G0} = 0$ V.

S2. TRANSFER CHARACTERISTICS

The transfer characteristics (I_{SD} vs V_G) of all eight devices were measured for different V_{SD} values. For D1, measurements were conducted at 8.5 K, with results shown in Fig. S1. For the remaining devices, measurements were conducted at 14 mK. Results for D4 are presented in Fig. 2a, while results for the other devices are shown in Fig. S2. D8 exhibited conductance resonances and plateaus likely due to quantum interference effects, possibly

coupled with ballistic transport modes (Fig. S2). Such behaviours are not captured by traditional FET models and thus D8 was excluded from analysis.

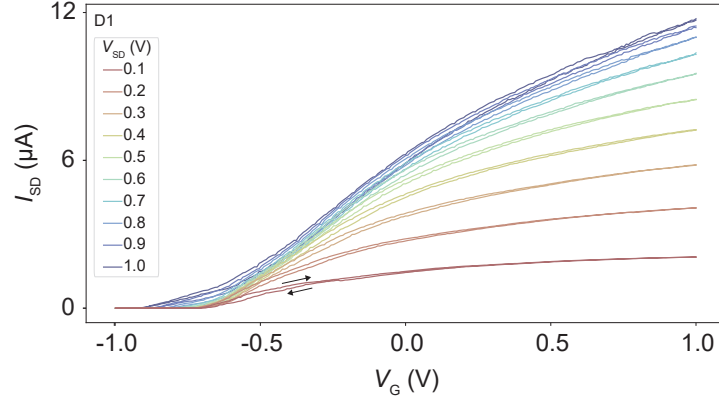


FIG. S1. Transfer characteristics of D1 measured at 7.5 K, for different values of V_{SD} , from 0.1 V (red) to 1 V (blue).

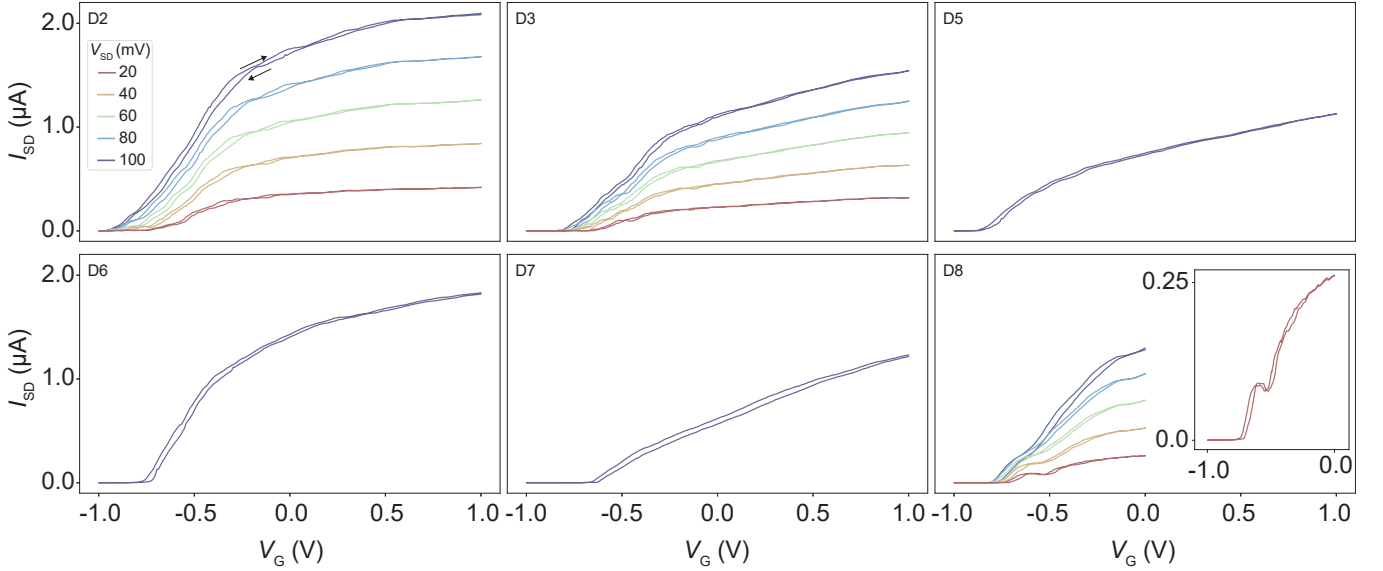


FIG. S2. Transfer characteristics of several devices measured at 14 mK, for different values of V_{SD} , ranging from 20 mV (red) to 100 mV (blue). D8 shows effects of quantum interference and ballistic transport at low bias.

S3. EXTRACTING THRESHOLD VOLTAGE AND MOBILITY

The threshold voltage and mobility were calculated following the procedure outlined in Ref. 32. First, the transfer curves, I_{SD} vs V_G , are normalized by the applied V_{SD} , yielding the conductance $G(V_G)$ (blue line in Fig. S3). The trans-conductance, dG/dV_G , is computed (yellow line in Fig. S3) and fitted with an asymmetric Lorentzian:

$$\frac{dG}{dV_G} = \frac{2A}{\pi U_0} \left(1 + 4 \left(\frac{V_G - V_{G0}}{U_0} \right)^2 \right)^{-1}, \quad (S1)$$

where

$$U_0 = 2c (1 + \exp(a(V_G - V_{G0})))^{-1}, \quad (S2)$$

and A , V_{G0} , c and a are fitting parameters (green line in Fig. S3). The coordinates of the Lorentzian peak are the gate voltage, V_{inf} , and the trans-conductance, $s_{inf} = dG/dV_G|_{V_G=V_{inf}}$, at the inflection point (green dots and dashed

lines in Fig. S3). With this information, the tangent line at the inflection point is:

$$T(G) = G_{\text{inf}} + s_{\text{inf}}(V_G - V_{\text{inf}}), \quad (\text{S3})$$

(purple line in Fig. S3) where $G_{\text{inf}} = G(V_{\text{inf}})$ (blue dot and dashed line in Fig. S3). The threshold voltage, V_{th} is, then, defined as the point where $T(G) = 0$ (purple dot and dashed line in Fig. S3), and the zero density voltage is defined as $V_{n=0} = V_{\text{th}} - 2|V_{\text{inf}} - V_{\text{th}}|$ (grey dashed line in Fig. S3).

Next, the series resistance, R_s , is estimated fitting the conductance to the Drude expression:

$$G = \left(R_{s, \text{fit}} + \frac{L^2}{\mu_{\text{fit}} C (V_G - V_{n=0})} \right)^{-1}, \quad (\text{S4})$$

where $R_{s, \text{fit}}$ and μ_{fit} are fitting parameters and L is the device length (red line in Fig. S3). In this step the starting point for the fit is fixed at $V_{\text{fit}} = V_{\text{inf}} + 2|V_{\text{inf}} - V_{\text{th}}|$ (red dashed line in Fig. S3).

Finally, the series resistance is subtracted from the total resistance to obtain the device conductance and extract the gate-dependent mobility, μ :

$$\mu(V_G) = \frac{L^2}{C(V_G - V_{n=0}) \left(\frac{1}{G(V_G)} - R_{s, \text{fit}} \right)}. \quad (\text{S5})$$

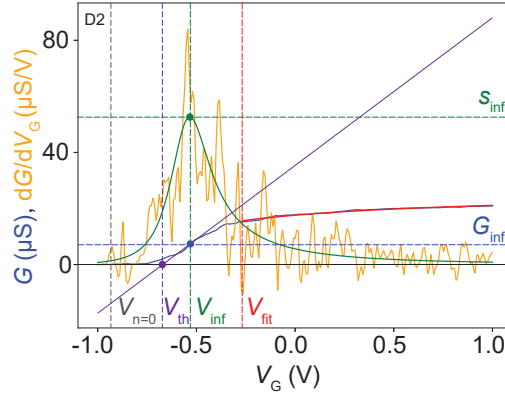


FIG. S3. Extracting the threshold voltage and mobility for D2 following the procedure outlined in Ref. 32. The conductance (blue line) is used to compute the trans-conductance (yellow line), which is fitted by an asymmetric Lorentzian (green line). The coordinates of the Lorentzian peak (green dot), V_{inf} and s_{inf} (green dashed lines), are used to compute the tangent to the conductance curve at inflection point (purple line). The threshold voltage, V_{th} , is defined as the point where the tangent line is zero (purple dot and dashed line) and the zero density voltage is defined as $V_{n=0} = V_{\text{th}} - 2|V_{\text{inf}} - V_{\text{th}}|$ (grey dashed line). The conductance is fitted to the Drude expression (red line), with the fit starting at $V_{\text{fit}} = V_{\text{inf}} + 2|V_{\text{inf}} - V_{\text{th}}|$ (red dashed line), to extract the series resistance, which is then used to compute the gate-dependent mobility shown in the main text, Fig. 2f.

S4. HYSTERESIS COMPUTATIONS

To evaluate the hysteresis we measure I_{SD} while sweeping V_G up ($I_{\text{SD}, \text{up}}$) and down ($I_{\text{SD}, \text{down}}$). We are interested in the V_G difference between the two sweeps as a function of I_{SD} . To compare the two curves, it is necessary to interpolate one of them so that both curves share the same I_{SD} values. We define $I_{\text{SD}} = I_{\text{SD}, \text{up}}$ so that $V_{G, \text{up}} = V_G$, and we interpolate the down-sweep measurement points to obtain $V_{G, \text{down}}$ as a function of I_{SD} (see Fig. S4a). Figure S4b shows $V_{G, \text{diff}} = (V_{G, \text{down}} - V_{G, \text{up}})$ for D4 and $V_{\text{SD}} = 40$ mV. This difference is nearly constant except at extreme I_{SD} where the transfer curves saturate. Therefore, it appears necessary to limit the evaluation of $V_{G, \text{diff}}$ to the region close to the inflection point of the transfer curve. This region is defined by fitting the derivative of the up-sweep transfer curve to an asymmetric Lorentzian, of the form described in equation S1 (Fig. S4c). We determine the two points on the asymmetric Lorentzian corresponding to half the peak value, V_{G1} and V_{G2} , which define $\text{FWHM}_{\text{AL}} = |V_{G2} - V_{G1}|$. The current values, I_{SD1} and I_{SD2} , corresponding to these voltages are used to delimit the range in which $V_{G, \text{diff}}$ is evaluated. The hysteresis parameter ΔV_G , discussed in the manuscript (Fig. 2e) is then defined as the maximum $V_{G, \text{diff}}$ in this range (Fig. S4b).

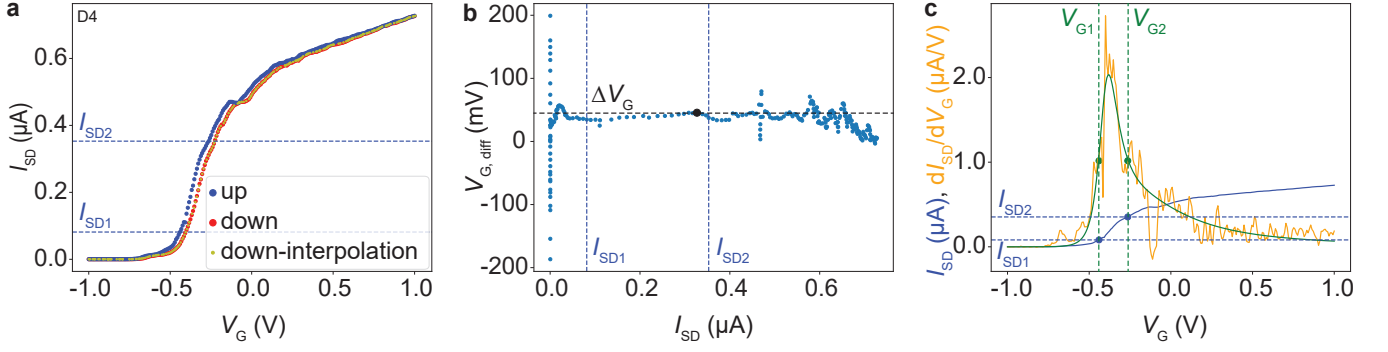


FIG. S4. **a** Transfer characteristics of D4 measured at $V_{SD} = 40$ mV and $T = 14$ mK, during an up (blue) and down (red) sweep. The down-sweep measurement points are interpolated to match the current of the up-sweep points (yellow). The blue dashed lines, I_{SD1} and I_{SD2} , represent the range in which ΔV_G is evaluated. **b** Voltage difference between the up and down sweep, $V_{G, \text{diff}}$, as a function of I_{SD} . ΔV_G is defined as the maximum $V_{G, \text{diff}}$ in the range limited by the blue dashed lines, I_{SD1} and I_{SD2} . **c** Derivative (orange line) of the up sweep transfer characteristics (blue line), fitted by an asymmetric Lorentzian (green line). V_{G1} and V_{G2} (green points and green dashed lines) define the full-width half-maximum. On the transfer characteristics, these corresponds to I_{SD1} and I_{SD2} (blue points and blue dashed lines), which determine the range in which ΔV_G is evaluated.

S5. BANDWIDTH MEASUREMENTS IN THE AMPLIFIER CONFIGURATION

To investigate the device bandwidth in the amplifier configuration with D1 shown in Fig. 3a we applied a sinusoidal input voltage at varying frequencies f :

$$V_{\text{in}} = V_0 + A_{\text{in}} \sin(2\pi ft + \phi_{\text{in}}), \quad (\text{S6})$$

where $V_0 = -0.882$ V is the optimal gate-operation point of the amplifier, $A_{\text{in}} = 0.01$ V is the amplitude, t is the time and ϕ_{in} is the phase. We fitted the measured V_{out} to a sine wave of the form:

$$V_{\text{out}} = A_{\text{out}} \sin(2\pi ft + \phi_{\text{out}}), \quad (\text{S7})$$

where A_{out} and ϕ_{out} are fitting parameters (Fig. S5a). The gain, A , was calculated as $A = A_{\text{out}}/A_{\text{in}}$. Figure S5b shows that A decreases with increasing f , starting from frequencies below 1 Hz, which is much lower than the RC filter cutoff frequency $f_c = 5$ kHz. This is due to the load resistance, $R_{\text{load}} = 100$ M Ω , which effectively reduce the cutoff frequency:

$$f_{c, \text{amp}} = \frac{1}{2\pi RC_f} = \frac{1}{2\pi(R_f + R_{\text{load}})C_f} = f_c \frac{R_f}{R_f + R_{\text{load}}} \approx 0.3 \text{ Hz}, \quad (\text{S8})$$

where $R_f \approx 6$ k Ω and C_f are the resistance and capacitance of the cryostat filters. Consequently, it is impossible to measure bandwidths higher than ≈ 0.3 Hz in the amplifier configuration, and, thus, the bandwidth is analyzed by studying the frequency response of the isolated NWFET.

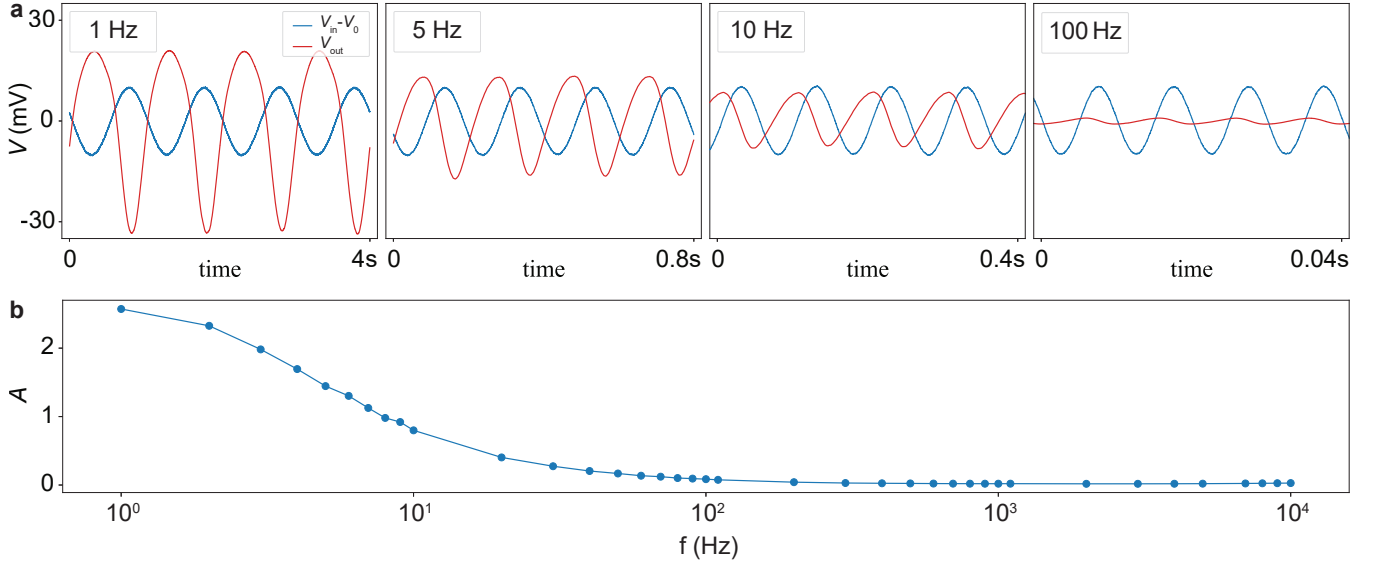


FIG. S5. **a** V_{out} response (red) to a sinusoidal V_{in} (blue) of different frequencies, for the amplifier configuration shown in Fig. 3a. **b** Frequency dependence of the gain, computed as the ratio of the amplitudes of the sinusoidal fit of V_{out} and V_{in} . The measurements are performed at 7.5 K.

S6. NWFET BANDWIDTH MEASUREMENTS

Similarly to what discussed in supplementary section S5, the bandwidth of the NWFETs is measured by applying a sinusoidal gate voltage:

$$V_G = V_{G0} + A_{V_G} \sin(2\pi f t + \phi_{V_G}), \quad (S9)$$

where $A_{V_G} = 20$ mV and V_{G0} varies depending on the device as described supplementary section S1. The measured I_{SD} is fitted to a sine wave of the form:

$$I_{SD} = A_{I_{SD}} \sin(2\pi f t + \phi_{I_{SD}}), \quad (S10)$$

as shown Fig. S6. If the fit has a coefficient of determination, R^2 , lower than 0.25, the dataset is excluded from the analysis. The frequency response is computed by normalizing the value of $A_{I_{SD}}$ by the value measured at the lowest frequency ($f_{min} = 1$ or 100 Hz):

$$I_{normalized}(f) = \frac{A_{I_{SD}}(f)}{A_{I_{SD}}(f = f_{min})}. \quad (S11)$$

Figure 3e shows $I_{normalized}$ as a function of f for various devices. The final signal at high frequency could be due to capacitive cross-talk of the cryostat wiring.

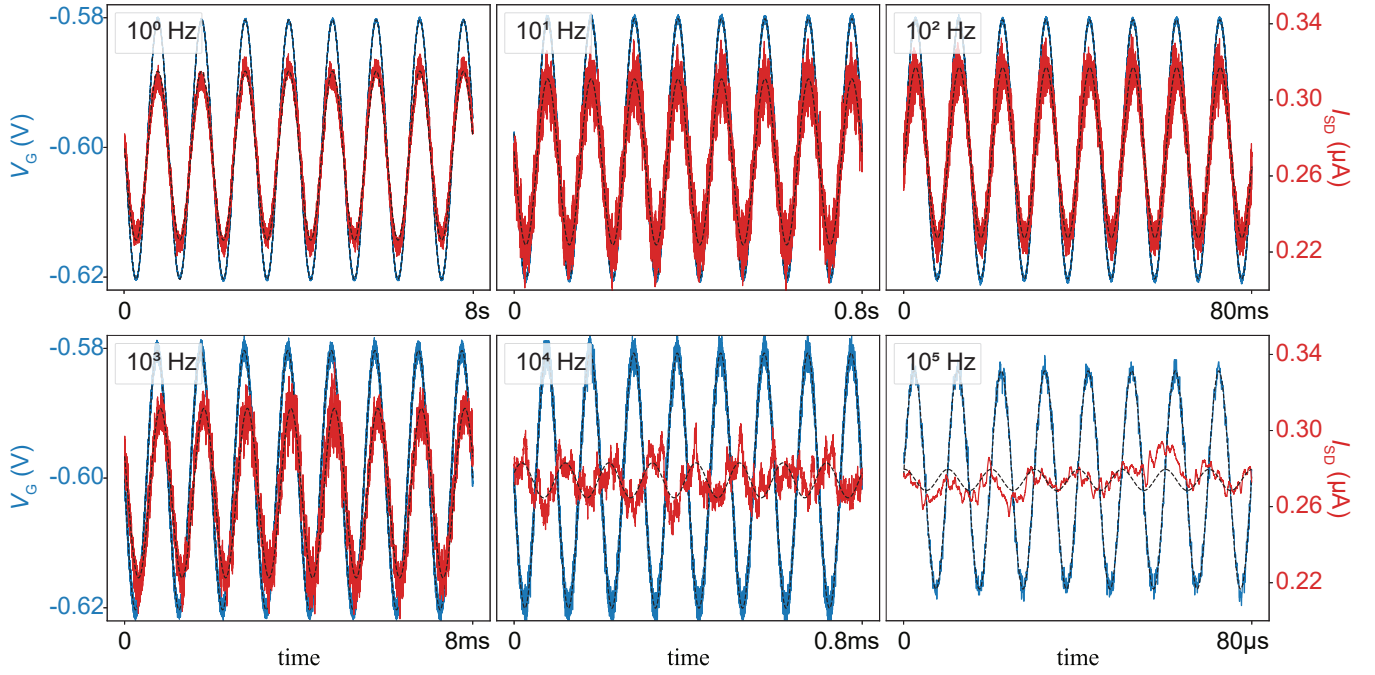


FIG. S6. Current response (red) to a sinusoidal gate voltage (blue) of different frequencies for device D3 at 1.2 K. The black dashed lines indicate the sinusoidal fits.

REFERENCES

- ¹M. Friedl, K. Cerveny, P. Weigele, G. Tütüncüoğlu, S. Martí-Sánchez, C. Huang, T. Patlatiuk, H. Potts, Z. Sun, M. O. Hill, L. Güniat, W. Kim, M. Zamani, V. G. Dubrovskii, J. Arbiol, L. J. Lauhon, D. M. Zumbühl, and A. Fontcuberta i Morral, “Template-Assisted Scalable Nanowire Networks,” *Nano Lett.* **18**, 2666–2671 (2018).
- ²F. Krizek, J. E. Sestoft, P. Aseev, S. Martí-Sánchez, S. Vaitiekėnas, L. Casparis, S. A. Khan, Y. Liu, T. Stankevič, A. M. Whiticar, *et al.*, “Field effect enhancement in buffered quantum nanowire networks,” *Phys. Rev. Mater.* **2**, 093401 (2018).
- ³S. Vaitiekėnas, A. M. Whiticar, M.-T. Deng, F. Krizek, J. E. Sestoft, C. J. Palmström, S. Martí-Sánchez, J. Arbiol, P. Krogstrup, L. Casparis, and C. M. Marcus, “Selective-Area-Grown Semiconductor-Superconductor Hybrids: A Basis for Topological Networks,” *Phys. Rev. Lett.* **121**, 147701 (2018).
- ⁴J. A. Del Alamo, “Nanometre-scale electronics with III–V compound semiconductors,” *Nature* **479**, 317–323 (2011).
- ⁵C. Zhang and X. Li, “III–V nanowire transistors for low-power logic applications: a review and outlook,” *IEEE Trans. Electron Devices* **63**, 223–234 (2016).
- ⁶A. W. Dey, C. Thelander, E. Lind, K. A. Dick, B. M. Borg, M. Borgstrom, P. Nilsson, and L.-E. Wernersson, “High-performance InAs nanowire MOSFETs,” *IEEE Electron Device Lett.* **33**, 791–793 (2012).
- ⁷A. C. Ford, J. C. Ho, Y.-L. Chueh, Y.-C. Tseng, Z. Fan, J. Guo, J. Bokor, and A. Javey, “Diameter-Dependent Electron Mobility of InAs Nanowires,” *Nano Lett.* **9**, 360–365 (2009).
- ⁸S. Sasaki, K. Tateno, G. Zhang, H. Suominen, Y. Harada, S. Saito, A. Fujiwara, T. Sogawa, and K. Muraki, “Encapsulated gate-all-around InAs nanowire field-effect transistors,” *App. Phys. Lett.* **103** (2013).
- ⁹S. A. Dayeh, E. T. Yu, and D. Wang, “Transport coefficients of InAs nanowires as a function of diameter,” *Small* **5**, 77–81 (2009).
- ¹⁰K. Storm, G. Nylund, L. Samuelson, and A. P. Micolich, “Realizing lateral wrap-gated nanowire FETs: controlling gate length with chemistry rather than lithography,” *Nano Lett.* **12**, 1–6 (2012).
- ¹¹H. A. Nilsson, P. Caroff, C. Thelander, E. Lind, O. Karlström, and L.-E. Wernersson, “Temperature dependent properties of InSb and InAs nanowire field-effect transistors,” *Appl. Phys. Lett.* **96** (2010).
- ¹²S. Dhara, S. Sengupta, H. S. Solanki, A. Maurya, A. Pavan R, M. Gokhale, A. Bhattacharya, and M. M. Deshmukh, “Facile fabrication of lateral nanowire wrap-gate devices with improved performance,” *Appl. Phys. Lett.* **99** (2011).
- ¹³Y. Jiang, R. Shen, T. Li, J. Tian, S. Li, H. H. Tan, C. Jagadish, and Q. Chen, “Enhancing the electrical performance of InAs nanowire field-effect transistors by improving the surface and interface properties by coating with thermally oxidized Y₂O₃,” *Nanoscale* **14**, 12830–12840 (2022).
- ¹⁴L. E. Froberg, C. Rehstedt, C. Thelander, E. Lind, L.-E. Wernersson, and L. Samuelson, “Heterostructure barriers in wrap gated nanowire FETs,” *IEEE Electron Device Lett.* **29**, 981–983 (2008).
- ¹⁵K. Blekker, B. Munstermann, A. Matiss, Q. T. Do, I. Regolin, W. Brockerhoff, W. Prost, and F.-J. Tegude, “High-frequency measurements on InAs nanowire field-effect transistors using coplanar waveguide contacts,” *IEEE Trans. Nanotechnol.* **9**, 432–437 (2010).
- ¹⁶L. Hofstetter, S. Csonka, J. Nygård, and C. Schönenberger, “Cooper pair splitter realized in a two-quantum-dot Y-junction,” *Nature* **461**, 960–963 (2009).

- ¹⁷T. S. Jespersen, M. Aagesen, C. B. Sørensen, P. E. Lindelof, and J. Nygård, “Tunable double dots and Kondo enhanced Andreev transport in InAs nanowires,” *J. Vac. Sci. Technol. B Microelectron. Nanometer Struct. Process. Meas. Phenom.* **26**, 1609 (2008).
- ¹⁸T. W. Larsen, K. D. Petersson, F. Kuemmeth, T. S. Jespersen, P. Krogstrup, J. Nygård, and C. M. Marcus, “Semiconductor-Nanowire-Based Superconducting Qubit,” *Phys. Rev. Lett.* **115**, 127001 (2015).
- ¹⁹S. Nadj-Perge, S. M. Frolov, E. P. A. M. Bakkers, and L. P. Kouwenhoven, “Spin-orbit qubit in a semiconductor nanowire,” *Nature* **468**, 1084–1087 (2010).
- ²⁰a. R. Wagner and s. W. Ellis, “Vapor-liquid-solid mechanism of single crystal growth,” *Appl. Phys. Lett.* **4**, 89–90 (1964).
- ²¹E. M. Freer, O. Grachev, X. Duan, S. Martin, and D. P. Stumbo, “High-yield self-limiting single-nanowire assembly with dielectrophoresis,” *Nature Nanotech* **5**, 525–530 (2010).
- ²²J. Yao, H. Yan, and C. M. Lieber, “A nanoscale combing technique for the large-scale assembly of highly aligned nanowires,” *Nature Nanotech* **8**, 329–335 (2013).
- ²³M. Fu, “Fabrication, Characterization and Parameter Extraction of InAs Nanowire-Based Device,” in *Electrical Properties of Indium Arsenide Nanowires and Their Field-Effect Transistors*, Springer Theses, edited by M. Fu (Singapore, 2018) pp. 31–51.
- ²⁴D. Olšteins, G. Nagda, D. J. Carrad, D. V. Beznasyuk, C. E. N. Petersen, S. Martí-Sánchez, J. Arbiol, and T. S. Jespersen, “Cryogenic multiplexing using selective area grown nanowires,” *Nat Commun* **14**, 7738 (2023).
- ²⁵M. Friedl, K. Cervený, C. Huang, D. Dede, M. Samani, M. O. Hill, N. Morgan, W. Kim, L. Guniat, J. Segura-Ruiz, *et al.*, “Remote doping of scalable nanowire branches,” *Nano Lett.* **20**, 3577–3584 (2020).
- ²⁶R. L. M. Op het Veld, D. Xu, V. Schaller, M. A. Verheijen, S. M. E. Peters, J. Jung, C. Tong, Q. Wang, M. W. A. de Moor, B. Hesselmann, K. Vermeulen, J. D. S. Bommer, J. Sue Lee, A. Sarikov, M. Pendharkar, A. Marzegalli, S. Koelling, L. P. Kouwenhoven, L. Miglio, C. J. Palmström, H. Zhang, and E. P. A. M. Bakkers, “In-plane selective area InSb–Al nanowire quantum networks,” *Commun. Phys.* **3**, 1–7 (2020).
- ²⁷L. Södergren, P. Olausson, and E. Lind, “Low-Temperature Characteristics of Nanowire Network Demultiplexer for Qubit Biasing,” *Nano Lett.* **22**, 3884–3888 (2022).
- ²⁸D. V. Beznasyuk, S. Martí-Sánchez, G. Nagda, D. J. Carrad, J. Arbiol, and T. S. Jespersen, “Scale-dependent growth modes of selective area grown III–V nanowires,” *Nano letters* **24**, 14198–14205 (2024).
- ²⁹D. V. Beznasyuk, S. Martí-Sánchez, J.-H. Kang, R. Tanta, M. Rajpalke, T. Stankevič, A. W. Christensen, M. C. Spadaro, R. Bergamaschini, N. N. Maka, C. E. N. Petersen, D. J. Carrad, T. S. Jespersen, J. Arbiol, and P. Krogstrup, “Doubling the mobility of InAs/InGaAs selective area grown nanowires,” *Phys. Rev. Materials* **6**, 034602 (2022).
- ³⁰F. Krizek, J. E. Sestoft, P. Aseev, S. Martí-Sánchez, S. Vaitiekėnas, L. Casparis, S. A. Khan, Y. Liu, T. Stankevič, A. M. Whitar, A. Fursina, F. Boekhout, R. Koops, E. Uccelli, L. P. Kouwenhoven, C. M. Marcus, J. Arbiol, and P. Krogstrup, “Field effect enhancement in buffered quantum nanowire networks,” *Phys. Rev. Materials* **2**, 093401 (2018).
- ³¹D. Olšteins, G. Nagda, D. J. Carrad, D. V. Beznasyuk, C. E. N. Petersen, S. Martí-Sánchez, J. Arbiol, and T. S. Jespersen, “Statistical Reproducibility of Selective Area Grown InAs Nanowire Devices,” *Nano Lett.* **24**, 6553–6559 (2024).
- ³²C. E. Petersen, D. J. Carrad, T. Désiré, D. Beznasyuk, J.-H. Kang, D. Olšteins, G. Nagda, D. V. Christensen, and T. S. Jespersen, “ $\mu_{2T}(n)$: A method for extracting the density dependent mobility in two-terminal nanodevices,” *arXiv preprint arXiv:2508.06173* (2025).
- ³³L. Olsson, C. Andersson, M. Håkansson, J. Kanski, L. Ilver, and U. O. Karlsson, “Charge accumulation at InAs surfaces,” *Phys. Rev. Lett.* **76**, 3626 (1996).
- ³⁴W. Yang, D. Pan, R. Shen, X. Wang, J. Zhao, and Q. Chen, “Suppressing the excess OFF-state current of short-channel InAs nanowire field-effect transistors by nanoscale partial-gate,” *Nanotechnology* **29**, 415203 (2018).
- ³⁵K. Tomioka, M. Yoshimura, and T. Fukui, “A III–V nanowire channel on silicon for high-performance vertical transistors,” *Nature* **488**, 189–192 (2012).
- ³⁶K. Tomioka, F. Izhizaka, and T. Fukui, “Selective-area growth of InAs nanowires on Ge and vertical transistor application,” *Nano Lett.* **15**, 7253–7257 (2015).
- ³⁷S. M. Sze, Y. Li, and K. K. Ng, *Physics of semiconductor devices* (John Wiley & sons, 2021).
- ³⁸T. Vasen, P. Ramvall, A. Afzalian, C. Thelander, K. Dick, M. Holland, G. Doornbos, S. Wang, R. Oxland, G. Vellianitis, M. van Dal, B. Duriez, J.-R. Ramirez, R. Droopad, L.-E. Wernersson, L. Samuelson, T.-K. Chen, Y.-C. Yeo, and M. Passlack, “InAs nanowire GAA n-MOSFETs with 12–15 nm diameter,” in *2016 IEEE Symp. VLSI Technol.* (2016) pp. 1–2.
- ³⁹C. Zhang, W. Choi, P. K. Mohseni, and X. Li, “InAs Planar Nanowire Gate-All-Around MOSFETs on GaAs Substrates by Selective Lateral Epitaxy,” *IEEE Electron Device Lett.* **36**, 663–665 (2015).
- ⁴⁰M. Fu, D. Pan, Y. Yang, T. Shi, Z. Zhang, J. Zhao, H. Q. Xu, and Q. Chen, “Electrical characteristics of field-effect transistors based on indium arsenide nanowire thinner than 10 nm,” *Applied Physics Letters* **105**, 143101 (2014).
- ⁴¹Q. Li, S. Huang, D. Pan, J. Wang, J. Zhao, and H. Q. Xu, “Suspended InAs nanowire gate-all-around field-effect transistors,” *Applied Physics Letters* **105**, 113106 (2014).
- ⁴²A. Beckers, F. Jazaeri, and C. Enz, “Theoretical limit of low temperature subthreshold swing in field-effect transistors,” *IEEE Electron Device Lett.* **41**, 276–279 (2019).
- ⁴³P. Sarangapani, Y. Chu, J. Charles, G. Klimeck, and T. Kubis, “Band-tail formation and band-gap narrowing driven by polar optical phonons and charged impurities in atomically resolved III–V semiconductors and nanodevices,” *Phys. Rev. Appl.* **12**, 044045 (2019).
- ⁴⁴T. Li, R. Shen, M. Sun, D. Pan, J. Zhang, J. Xu, J. Zhao, and Q. Chen, “Improving the electrical properties of InAs nanowire field effect transistors by covering them with Y2O3/HfO2 layers,” *Nanoscale* **10**, 18492–18501 (2018).
- ⁴⁵H. Riel, L.-E. Wernersson, M. Hong, and J. A. del Alamo, “III–V compound semiconductor transistors—from planar to nanowire structures,” *MRS Bulletin* **39**, 668–677 (2014).
- ⁴⁶N. Wang, X. Yuan, X. Zhang, Q. Gao, B. Zhao, L. Li, M. Lockrey, H. H. Tan, C. Jagadish, and P. Caroff, “Shape engineering of InP nanostructures by selective area epitaxy,” *ACS nano* **13**, 7261–7269 (2019).